THz Emission from metallic bilayers

Internship report by

Vito Volpe

for the Degree

in

M2 Quantum Devices / Nanotechnologies for ICT

A.Y. 2017/18

Internship advisors:
Dr Henri Jaffrès (UMφ)
Dr Paolo Bortolotti (Thales TRT)
Dr Sukhdeep Dhillon (LPA-ENS)

Academic advisors:
Dr Maria Luisa Della Rocca
Dr Fabrizio Pirri

Universitè Paris 7 Diderot

Paris, France

Politecnico di Torino

Torino, Italia

Thales R & T

Palaiseau, France

CNRS

Palaiseau, France

Acknowledgments

This report describes the work performed during my internship started in March 2018 at ”Unité Mixte de Physique Thales / CNRS” (UMR), Palaiseau, in agreement with academical institutions (”Universitè Paris 7 Diderot” and ”Politecnico di Torino”) and in collaboration with Laboratoire Pierre Agrain (LPA-ENS). This research unit is placed into the research centre of Thales Research & Technology, that counts in total about 350 employees, 80 doctorants and 100 scientists coming from partner research institutions. The UMR137 (UMφ) was created in 1995 by CNRS and Thales group (Thomson CSF at that time) involving also academic researchers from Université Paris Sud and, now, Université Paris Saclay. It has been directed by Alain Friederich until 2007 then Dr Frédéric Nguyen Van Dau become director in 2007 and always under the scientific supervision of Dr Albert Fert, winner of the Nobel Prize in 2007 for the dicovery of Giant Magnetoresistance (1988). The lab has three principal research themes: spintronics and nanomagnetisme, functional oxides and Superconducitivity at high temperature. This internship takes place is the spintronics group under the supervision of Dr Henri Jaffres (CNRS) and Dr Paolo Bortolotti (Thales) as well as Dr S. Dhillon (LPA-ENS) and Thi Huong Dang (post-doc). The spintornics group is interested right now in the study of novel interfacial effects between magnetic and non-magnetic materials involving Spin Hall Effect properties as well as novel interfacial effects due to the so called topological insulators, studied for their properties of spin-to-charge conversion (this new field of research is called ’spinorbitronics’).
My work mainly took place at Palaiseau with a part of time spent at Laboratoire Pierre Agrain in Paris, in the Ultrafast Spectroscopy Group concerning Time Domain Spectroscopy measurements.

Abstract

It was recently reported that THz emission can be realized in heterostructures composed of ferromagnetic and non-magnetic metal thin films via dynamical spin-to charge conversion. This occurs from interfacial Rashba spin-orbit coupling or inverted spin-Hall effect (ISHE) and evidenced via time-dependent spectroscopy [1–3]. This particular work and objectives focus on last results of THz emission provided by optimized growth bilayers composed of a high-spin orbit material and a ferromagnetic layer Co/Pt in different configurations by inserting gold, titanium and ruthenium thin layers for better electronic matching. Those bilayers state-of-the-art analysis is based on experiments combining RF-spin pumping and spin-to-charge conversion by ISHE [4, 5]. The THz experiments consist in exciting magnetization and spin-currents within the FM layer via femtosecond laser excitation and measuring, in the picosecond timescale, the relaxation of the correlated spin and charge currents responsible for THz dipolar emission. The advantages of the THz emitter based on magnetic heterostructures are low-cost and the polarization of emitted THz wave being easily tuned with an external magnetic field. Particular interesting are the results for the configuration Co/Pt/Au:W for which the THz signal is higher with respect to Co/Pt, even if the ISHE signal is still larger for the latter. To understand this point, it will be important to discuss the role of the generalized spin-mixing conductance. THz signals strongly depend on the spin Hall angle of non-FM metal, spin diffusion length, and spin-mixing conductance. Since in this work spin hall angle and spin diffusion length are considered as constants, mainly because the non-magnetic material is always the same (Pt), it should be possible to find that in the structures with large spin-mixing conductance or larger spin transmission the THz signal becomes higher. My internship work and present report mainly demonstrate that FMR-ISHE experiment becomes a relative fast and reliable method to study THz emission for these spintronic samples and to predict possible optimizations.

Contents

CHAPTER 1

Introduction

The report is organized in five chapters: 1) introduction to underline objectives of this internship and explain the basic theoretical background; 2) where different used setup are described; 3) to show all the results and their analysis, 4) regarding theory and simulations and 5) with conclusions.

1.1 The reasons for THz and Objective of the work

THz photonics is an active research area (with many very recent conferences concerning THz-spintronics from UMφ-CNRS Thales and Lpa-ENS partners as [6–8]) where new sources and detectors are actively sought for a range of applications. THz waves cover the emission gap from the Infrared to the microwave frequencies and correspond to an electromagnetic spectral range from 0.1 to 30 THz. This range concides with many fundamentals resonances of materials, since bonding energies of many large molecules are in the same energy range of THz waves (from 0.5 to 120 meV). For this reason THz spectroscopy can be applied to material composition analysis, important for chemical, biological and medical applications [9].
Moreover THz waves possess a strong potential to study the matter-light interactions, to be used for imaging and safety systems [10]. Their propagation properties depend also on the conductivity of materials, leading to another possible use of THz spectroscopy to perform conductivity measurements in a non-destructive and non-invasive method [11].
Up to now, the optical rectification from electro-optical crystal, transient of electrical current in semiconductor antennas and air plasmas induced by femtosecond laser beams the most famous methods to generate THz waves. In the last years a new type of THz source was explored constituted by a multilayer system of magnetic and nonmagnetic layers [1–3]. In this context, Co/Pt interfaces or derived combination materials (like CoFeB/Pt) represent actually the best systems for THz emission able to exceed actual performances of ZnTe electro-optical crystals. This very interesting feature can be correlated to the very large spin-mixing conductance measured in several groups (fig 1.1) from FMR spin-pumping data from the extraction of the FMR linewidth. It results in an efficient THz emission mainly because excited majority spins enter freely in the Pt (spin-orbit material) without any reflections which are generally accompanied with spin-flips and nor

spin-to-charge conversion events necessary to produce electric-field emission. This makes strong advantages or Co/Pt family over other couples of bilayers (e.g. NiFe/Au:W) [12].

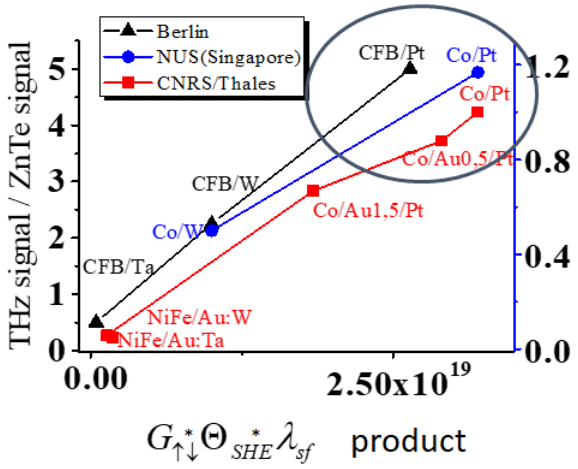

FIGURE 1.1 Correlation between THz signal and product among spin mixing conductance, Spin Hall angle (SHA) and spin diffusion length for different bilayer systems explored by the main groups worldwide

However, on the other hand, it is well admitted today that the Co/Pt interface is far from being optimal from spin-to-charge conversion point of view or local spin-decoherence by local spin-precession. Indeed, since the recent work of JC Rojas-Sanchez et al [4], it is well know that this specific interface introduces a strong discontinuity of the spin-current (or spin-loss) due to the carrier crossing through evanescent interface state produced by a strong spin-orbit field (Rashba field). This Rashba field, generally explored by spin pumping experiments (FerroMagnetic Resonance and Inverse Spin Hall Effect esperiments) [4], has for effect to introduce decoherence in the longitudinal component of the spin-injected from Pt, leading to a decrease by a factor between 2 and 3 of the spin-conversion. The more the spin-orbit field is important, the larger is the decoherence and the strongest the spin loss and spin-charge conversion.

Starting from those observations, one master idea is to increase the effective spin-transmission (decrease of the spin-memory loss) by making a precise engineering of the interface, at the atomic scale, by inserting some layers of atoms neutral from the point-of-view of spin-orbit. The constraint is to maintain the very large spin-transmissivity of Co/Pt with the need to avoid a too thick deposition typically over 1 or 1.5 nm ([4]).

In this work:

1) first approach is to use Au insertion (or Au:W small percentage) in the 0.2-1.5 nm range to reduce the interfacial Rashba strength. This is because Au is expected to be more neutral than Pt because the carrier density-of-state at the Fermi level does not possess d-electrons but simply s-electrons. This is the starting point of this internship and results presented here are very convincing from the spin-pumping FMR point-of-view and correlation with the THz signal will is present;

2) the second possibility is to investigate are Co/Pt bilayers with Ti insertion as demonstrated recently in a group in Korea ([13]) showing up a decrease of the spin-mixing conductance together with an increase of the ISHE in Pt after Ti insertion. The same effect with Au is expected and it could be linked to the decrease of spin-orbit field by atomic insertion;
3) The third idea and novelty of this work is the possibility to increase the spin-transmission and THz emission in the Co/Pt family by using a back spin absorber in trilayer systems of the type Co/Pt/X. X (=AuW, Ru) plays here the role of a local very thin spin-absorber able to decrease the majority-spin-current at the second interface and then enlarge the overall oscillator dipole amplitude.

We introduce now the main theoretical background concerning spin pumping, FerroMagnetic Resonance and THz methods needed for analysis.

1.2 Theoretical Background

The structure we want to study is a multilayer composed by a ferromagnetic material and a normal metal. The basic idea is to pump spin current from the ferromagnet to the normal metal, this spin current will diffuse in the normal metal and thanks to Inverse Spin Hall Effect there is a transient for the charge current leading to the production of THz signal.

1.2.1 Magnetization Precession and Spin pumping

If we consider a ferromagnetic material within an external magnetic field ($\mathbf{H}_{ext}$) it feels an effective magnetic field $\mathbf{H}_{eff}$ that includes not only the external field but also the inner field caused by the electron spin system we are considering. A ferromagnet has its own total magnetic moment $\mathbf{M}$ so there is the creation of a torque $\mathbf{T} = \mathbf{M} \times \mathbf{H}_{eff}$. The presence of a torque causes the precession of the angular momentum $\mathbf{L}$:

$$\frac{d\mathbf{L}}{dt} = \mathbf{T} = \mathbf{M} \times \mathbf{H}_{eff}$$

But it's also true that, given $\gamma = \frac{e}{m_e}$ the gyromagnetic ratio, the total magnetic momentum is $\mathbf{M} = \gamma \mathbf{L}$ and so there is a precession for $\mathbf{M}$ too:

$$\frac{d\mathbf{M}}{dt} = \gamma \cdot \frac{d\mathbf{L}}{dt} = \gamma[\mathbf{M} \times \mathbf{H}_{eff}]$$

This is the Larmor equation and it describes an undamped precession of the magnetization about the effective magnetic field. The term "undamped" is used because the precession-cone angle (the angle between $\mathbf{H}_{eff}$ and $\mathbf{M}$) and the magnitude of the magnetization are constant during the process. In this way the energy, given by the scalar product of effective magnetic field and the magnetization, has not a minimum but remains constant and this doesn't make any sense because for a ferromagnetic material it's known that the total magnetic momentum tends to align itself following

the direction of the effective magnetic field (phenomenon called Magnetization 'relaxation'). This means that there is an additional torque to take into account. The realistic equation is the Landau-Lifshitz-Gilbert (LLG) equation:

$$\frac{d\mathbf{M}}{dt} = \gamma[\mathbf{M} \times \mathbf{H}_{eff}] + \frac{\alpha}{|\mathbf{M}|}\Big[\mathbf{M} \times \frac{d\mathbf{M}}{dt}\Big] \tag{1.1}$$

where the second term of the equation induces a damped precession mechanism in which the precession-cone angle and the magnetization's magnitude are no more constants. In particular α is the so called "Gilbert" damping parameter. Since we can't know exactly what is the effective field we will fix H_{ext} and we consider an effective magnetization M_{eff} that will be calculated in Ferromagnetic Resonance.

On the other hand, it has been demonstrated ([14]) that motion of the magnetization in a ferromagnet can emit a spin current into an adjacent conductor. This process is called **Spin Pumping**. By considering the Stoner model at equilibrium in a ferromagnet there are two separate bands for up and down spins split by the exchange energy. If the magnetization's direction changes then the bands shift in energy and to come back to the equilibrium position there must be a spin transfer from one band to the other. This process, called "spin relaxation", can happen within the ferromagnet or in the vicinity of an adjacent layer that behaves as a recevoir to which spins can be transfered into. In particular the spin current density through the ferromagnet/normal interface is ([5]) :

$$\mathbf{j}_s^{pump} = \frac{\hbar}{4\pi} g_r^{\uparrow\downarrow}(\mathbf{m} \times \dot{\mathbf{m}}) + \frac{\hbar}{4\pi} g_i^{\uparrow\downarrow}\dot{\mathbf{m}}$$

where $\mathbf{m}$ is the unit vector along the magnetization, $\dot{\mathbf{m}}$ is the first derivative in time of $\mathbf{m}$ and $g^{\uparrow\downarrow}$ represent the spin mixing conductance at the interface (with indices r and i for the real part and imaginary part respectively). The spin current enters in the normal material producing a spin accumulation that causes a back flow spin current density. This effect can be taken into account by renormalizing the value of the spin mixing conductance into an effective one so that:

$$\mathbf{j}_s^{F/N} = \mathbf{j}_s^{pump} - \mathbf{j}_s^{back} = \frac{\hbar}{4\pi} g_{r,eff}^{\uparrow\downarrow}(\mathbf{m} \times \dot{\mathbf{m}}) + \frac{\hbar}{4\pi} g_{i,eff}^{\uparrow\downarrow}\dot{\mathbf{m}}$$

Then it's possible to omit the imaginary part of the effective spin mixing conductance because it's much smaller than the real part for pure mettalic species. This expression underlines the fact that the direction of the spin current is perpendicular with respect to the plane of both magnetization and his first derivative. Spin current posses three components, one perpendicular and two parallels with respect to the interface. The average over time is constant for spin current components parallel to the interface: $\mathbf{j}_{s,DC}^{F/N} = \frac{\hbar}{4\pi} g_{r,eff}^{\uparrow\downarrow} \sin^2\theta$ where θ is the cone precession angle and ω is the precession frequency. In order to make the total average over time of total spin current at the interface further steps are necessary: in particular it must be considered the Landau-Lifshitz-Gilbert (LLG) equation with the introduction of a microwave field $\mathbf{h}_{rf}$ that produces a precession magnetization $\mathbf{m}_{rf}$ around

the equilibrium position $\mathbf{m}_0$. Then by using polar coordinates and substituting in the LLG equation it's possible to extract the expression for the susceptibility χ and the one for the average value for the spin current $< \mathbf{j}_s^{F/N} >$.

1.2.2 Inverse Spin Hall Effect

The inverse spin Hall effect consists in the production of a charge current from a spin current with its own polarization via spin-orbit interaction (SOI). In a normal conductor the two populations are splitted in the same direction because of scattering processes that include SOI. This means that there is a non-zero electron motion in one side of the material, a charge current is produced ($\mathbf{J}_c$). The scattering mechanisms are skew scattering and side jump scattering: in the first case the electron's scattering probabilities with a strong SOI scattering center are different in the possible direction depending on the spin orientation of the electron itself; in the second case potential of the scattering center changes depending on the spin orientation of the incoming electron leading to different spatial displacements. The net charge current density is ([5]):

$$\mathbf{j}_{c,ISHE} = \frac{2e}{\pi}\theta_{SHE}\mathbf{z} \times \mathbf{j}_s$$

where $\mathbf{z}$ is the spin current flow direction, θ_{SHE} is the spin Hall angle, a parameter that evaluate how efficient conversion from spin current into charge current is, $\mathbf{j}_s$ is the spin current vector that has the direction of the polarization and it depends on both spatial coordinate z and time. This expression is useful to get the total charge current produced with Inverse Spin Hall Effect by taking the average over time of spin current and integrating in the z direction. Once the total charge current is known the electric field and the elctromotive force V_{ISHE} can be computed. This quantity is important because it's the measured one.

1.2.3 Laser induced ultrafast spin transport

Now a description of fundamentals of laser induces ultrafast spin transport follows.
To produce the THz signal a femtosecond laser is used to excite electrons in ferromagnetic material. Electron's lifetimes in ferromagnet depend on both energy and spin orientation. This means that when the laser excites the electrons there is an ultrafast flow of spin polarized electrons that leads the injection of a highly polarized spin current in nonmagnetic layer [15]. The situation is well represented in fig1.1. In the following experiments dealing with Thz emission, only laser excitations effects will be considered for spin currents. This generalizes the previous studies about beahvior of local magnetization under such laser excitations [16].

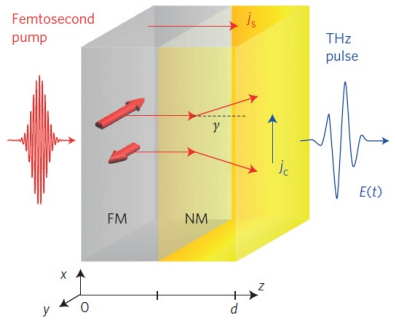

FIGURE 1.2 Representation of the situation that combine the fs laser excitation, ISHE and Thz emission. Picture from [2]

Now focus turns on description of interfacial spin orbit effects at interaface.

1.2.4 Spin Orbit Transport at Interface

The considered structure is a bilayer of nonmagnetic and ferromagnetic materials. The spin current is induced in the ferromagnetic material and it flows in direction perpendicular to the interface. This allows the use of CPP model ([17]) for spin current density $\mathbf{j}_s$. Once the spin current pass through the inferface into the nonmagnetic material there is spin to charge conversion thanks to Inverse Spin Hall Effect and the charge current has a direction parallel to the interface. The situation is different in bulk with respect to the region close to interface. In particular in bulk it's possible to use the spin dependent Boltzmann diffusive equation in steady state regime

$$v_z \frac{\partial g_s}{\partial z} + \left(\frac{1}{\tau_s} + \frac{1}{\tau_{sf}}\right) g_s = v_z \frac{\partial \bar{\mu}_s}{\partial z}(z) + \frac{\bar{\mu}_s - \bar{\mu}_{-s}}{\tau_{sf}}$$

where g is the difference between the fermi surfaces with spin accumulation and spin current (f) and at equilibrium (f_0), τ_s is the spin lifetime, $\frac{1}{\tau_{sf}}$ is the spin-flip rate, v_z is the carrier velocity and $\bar{\mu}_s$ is the spin accumulation. This equation can be applied in the regions far from the interface in both ferromagnetic and nonmagnetic materials with their different properties. Without taking into account the spin orbit interaction at interface and applying the diffusion equation to extract the spin current density behavior in space and it results to be continous at interface. Including the SOI the situation changes and in particular there is a discontinuity for the spin current density. This effect is also called 'Spin memory loss' and this will be demonstrated in chapter 4 numerically. To better and quickly understand the causes of this phenomenon one way is to come back to Hamiltonian expressions in the different regions:

$$H_{NM} = \frac{\hbar^2 k^2}{2m} + V_{NM} \tag{1.2}$$

$$H_{FM} = \frac{p^2}{2m} + V_{FM} - J_{exc}\mathbf{m} \cdot \hat{\sigma} \tag{1.3}$$

$$H_s = \frac{\hbar^2}{m} k_{so}(\mathbf{n}_{so} \cdot \hat{\sigma})\delta(x) = \mathbf{U} \cdot \hat{\sigma}\delta(x) \tag{1.4}$$

where eq 1.2 is the Hamiltonian in nonmagnetic material where there is a single wavefunction with one particular wavevector, eq 1.3 is the Hamiltonian in ferromagnetic material side where there is not one wavefunction but a spinor with the presence of two different wavectors depending on spin orientation. This is the starting point of calculations so treatment will be continued in chapter 4, focused on theory and simulations.

CHAPTER 2

Experimental setup

In this part, I will describe different experimental setup used during my internship, with which I have familiarized. Three types of set up are used: one for Ferromagnetic Resonance (FMR), one for Inverse Spin hall Effect and one for THz measurements.

2.1 FMR setup

For ferromagnetic resonance the idea is to use magnets to produce an external field for the sample. The multilayer sample is placed on a coplanar waveguide (CPW) in which a microwave field is injected and fixed in between the two magnetic poles. The external field produce a splitting of the energy states of the sample due to Zeeman effect. This energy splitting increases by increasing the magnetic field and it allows the possibility to absorb a part of the incident microwave power. The power depends on the frequency and so by working at higher frequencies the absorption occurs with higher splitting energy (reached at higher external magnetic field). The idea is to set the parameters of the injected microwave power in the CPW and to measure the transmitted power. To do those things two more instruments are used:

- the signal source ROHDESCHWARTZ SMF100A to inject the microwave signal throught the CPW
- lock-in aplifier model SR830DSP to collect the ouput signal and have a better signal to noise ratio.

In particular with this technique it's possible to measure the first derivative of the susceptibility's imaginary part χ'' with respect to the variation of magnetic field. To do that the trick is to introduce a modulation of the applied magnetic field. By this way it's possible to evaluate magnetic resonance properties and extract data which are useful to calculate the Gilbert damping constant and the effective magnetization [18], as it will be shown in section 3.1.

2.2 ISHE setup

The setup for the inverse spin Hall effect is an extension to the one used for FMR with small variations. The sample stuck on the CPW and gold deposition on the edges of it is performed to have contacts (with samples cut in bars). In such experiments, we measure the voltage between this two contacts that corresponds to the potential difference created by the accumulation of charge on one side of the sample due to spin-charge conversion (Inverse spin hall effect). Also in this case microwave power is injected into the CPW but in pulse mode. The lock in receives the output signal from the contacts and the reference signal from the signal source to extract the final signal with higher SNR.

2.3 Setup for THz

THz signal from bilayer or trilayer samples is obtained by performing the time domain spectroscopy (TDS) at Laboratoire Pierre Agrain (LPA) in Paris. A Titanium:Sapphire (Ti:Sa) laser with 100fs pulses running at 76MHz and an average power of 210mW (corresponding to 23 µJ/cm2 with a spot diameter of around 0.11 mm) is used to excite the spin-based structures to generate THz pulses. The emission is collected and focused in a reflection geometry using a set of parabolic mirrors. Electro-optic sampling was used to detect the THz radiation using a 0.5mm thick <110> ZnTe crystal and a low power probe beam from the Ti:Sa laser. Finally a delay line is used on the probe beam to map out the THz electric field as a function of time. The optical pump used for the excitation of the sample is mechanically chopped at 6700 kHz for lock-in detection. The THz TDS system is enclosed in a dry environment with a humidity level around 2% to reduce the effect of water absorption in air.

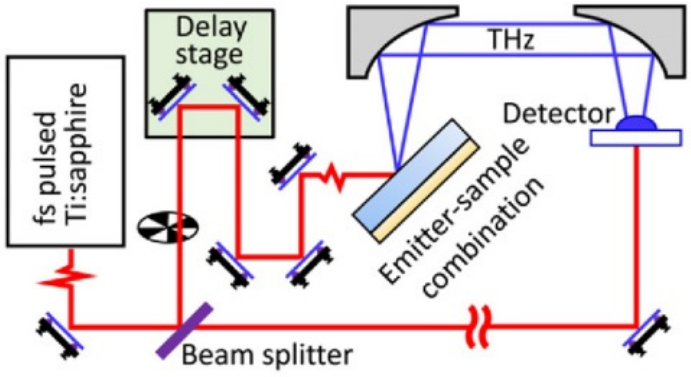

FIGURE 2.1 Scheme of TDS setup taken from [10]

CHAPTER 3

Experimental results

This chapter deals with experimental results obtained from spin pumping and THz measurements on different series of samples.
In relationship to objectives discussed above different samples have been produced in order to find an optimization for THz emission by comparing several proposal with respect to reference bilayer system made of Cobalt (Co) as ferromagnetic material and Platinum (Pt) as nonmagnetic material. An idea could be to insert an intermediate layer as Gold (Au) or Titanium (Ti, [13]) monolayer in it in order to reduce Rashba effect at interface and spin memory loss mechanism. Another idea could be to insert Au as third layer in order to optimize spin current profile in Pt layer when the Inverse Spin Hall effect takes place. For all types of samples different thickness of the additive layer are realized. Fabrication process is the magnetron RF sputtering performed at Palaiseau by Mme Sophie Collin.

3.1 Bilayer Co/Pt with insertion of Au

The first family of samples deals with bilayer Co/Pt with the Au insertion in between. The idea behind this choice is to modulate spin orbit Rashba interactions at the interface thanks to the presence of Au, thus reducing the role of d-electrons of the heavy 5d-metal. In this case the spin diffusion length inside Au is high and spin current injected from Co can reach the Pt where the Inverse Spin Hall Effect takes place. We have several samples with different Au thicknesses to see how the situation changes. In particular we have samples with Co thickness of 2 nm for THz measurements and Co thickness of 10 nm to perform the FMR and ISHE measurements, the Pt thickness fixed at 4 nm and Au layer with thicknesses of: 0.2 nm, 0.5 nm, 1 nm and 1.5 nm. As an example the FMR signal for Co(10nm)/Au(0.2nm)/Pt(4nm) is the following (fig 3.1):

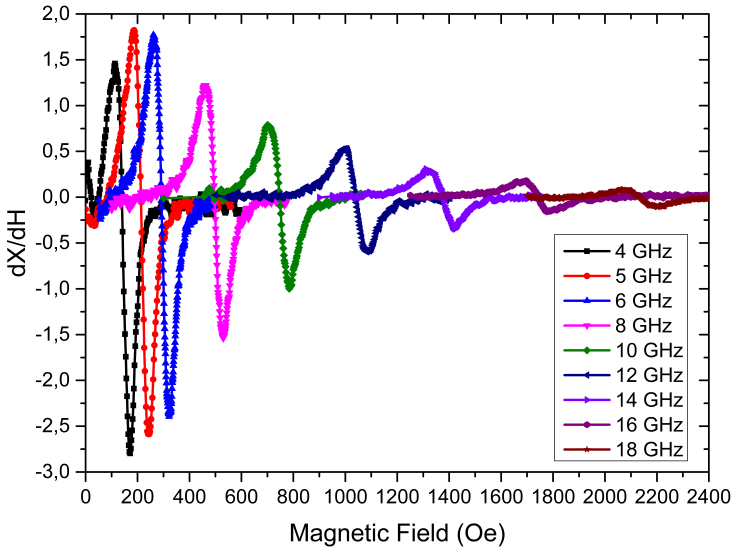

FIGURE 3.1 FMR emission for Co/Au(0.2nm)/Pt sample at several frequencies

From this results it's possible to extract the values of effective magnetization and Gilbert damping parameter, in terms of $\Delta\alpha = \alpha_{sample} - \alpha_{Co}$ [18]. In particular the damping $\Delta\alpha$ is obtained by the behavior in frequency of the parameter ΔH_{pp}, that is the difference in magnetic field between maximum and minimum of the first derivative of imaginary part of susceptibility. The relationship is linear [18], the width of the resonance increases with frequency of the injected microwave power.

$$\Delta H_{pp}(f) = \Delta H_0 + \frac{4\pi\hbar}{\sqrt{3}\cdot g_L \cdot \mu_B}\Delta\alpha \cdot f \tag{3.1}$$

where g_L is Landé factor, μ_B is Bohr magneton, f is the woking frequency and ΔH_0 indicate value of ΔH at zero frequency. For the previous measurements it is so possible to extract the damping value by making a linear interpolation (fig 3.2).

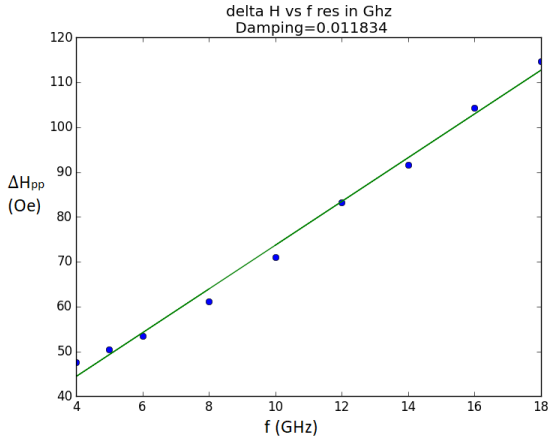

FIGURE 3.2 Linear fit from FMR results, on x there are frequencies in GHz, on y there are ΔH in Oe

The damping factor is represented in the slope as it's possible to understand from formula 3.1 . This procedure has been repeated for each sample of the series in order to obtain the data collected in the following table(table 3.1). The reference sample is the bilayer Co/Pt without Au insertion.

TABLE 3.1 Values extracted from FMR measurements

Au thickness (nm)	Damping value $\Delta\alpha$ (nm^{-2})	M_{eff} (emu/cm^{-3})	$\Delta\alpha \cdot M_{eff}$
$0(reference)$	0.01088 ± 0.000312	1565.404895	$17.03160526 \pm 0.488406327$
0.2	0.011834 ± 0.000382	1319.607203	$15.61623164 \pm 0.50408995$
0.5	0.009587 ± 0.000218	1636.240947	$15.68664196 \pm 0.356700526$
1	0.006865 ± 0.000257	1662.847934	$11.41545107 \pm 0.427351919$
1.5	0.005771 ± 0.000424	1709.384734	$9.8648593 \pm 0.724779127$

The results are the following: increasing the thickness of Au insertion the Gilbert damping parameter decreases and the effective magnetization increases but the product of the two factors decreases also. This is an important feature to consider because the spin mixing conductance is directly proportional to this product, as shown here [4]:

$$g_{eff}^{\uparrow\downarrow} = \frac{4\pi t_{Co}}{g\mu_B} M_{eff} \cdot \Delta\alpha \tag{3.2}$$

The next step is to measure the ISHE signal to check that the spin-to-charge conversion really occurs for all samples and how this signal changes from one sample to the other. As an example we show the real measurement for the reference bilayer and the fitting curve (figure 3.3) with the following fitting function:

$$V(H) = V_{offset} + V_{sym}\frac{\Delta H^2}{(H - H_{res})^2 + \Delta H^2} - V_{asym}\frac{\Delta H(H - H_{res})}{(H - H_{res})^2 + \Delta H^2} \tag{3.3}$$

where V_{sym} is the symmetric part of the signal (symmetrical in shape with respect to the resonant field H_{res}), V_{asym} is the asymmetric part of the signal , ΔH is the width of the signal and V_{offset} is a possible offset to be subtracted from the real signals . The approximation is to consider that Inverse Spin Hall effect signal is the only contribution to the symmetric part, by neglecting the rectification effects due to the anisotropic magnetoresistance (AMR) that instead may become important, together with the heating effect, and represented in the asymmetric component of the signal [5].

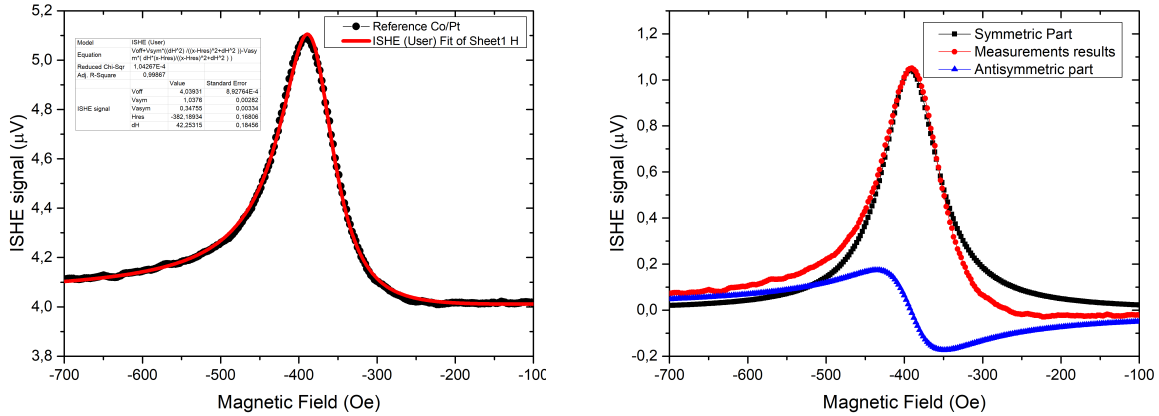

FIGURE 3.3 ISHE signal for the reference Co(10nm)/Pt(4nm): measurement results and fitting curve on left panel, symmetric and asymmetric components on left panel

Since the interesting part of the signal is in the symmetric component two different plots for all samples are shown: in the first one there are the real measurements and in the second one just the symmetric parts normalized with a fixed resonant magnetic field appear in order to have a direct idea of signal amplitudes for the several samples.

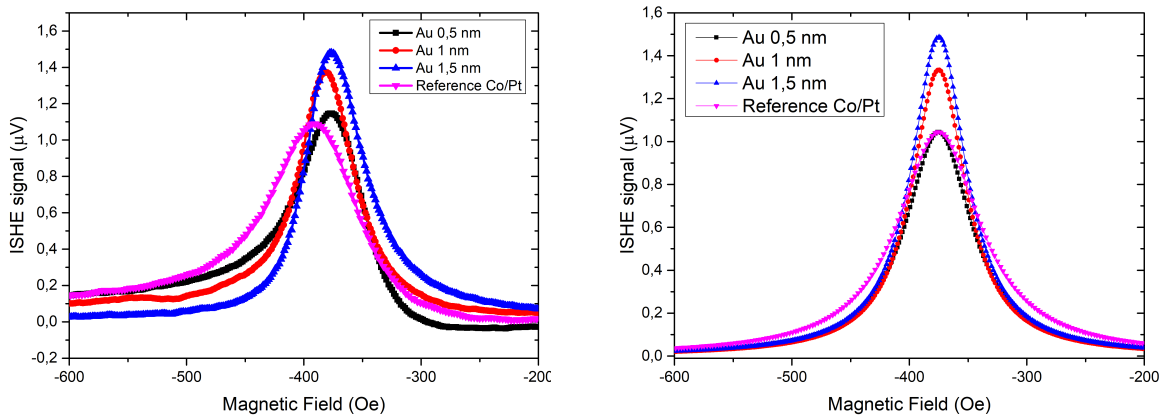

FIGURE 3.4 ISHE signal for the Au sample series

These plots (fig 3.4) show that ISHE signal amplitude increases with the Au thickness. This result can be compared with previous work of Lee group in Korea [13] in which they show a similar behavior of the signals by increasing the Ti thickness in between CoFeB/Pt heterostructures (same family if Co/Pt used for this work) and maybe it could be ascribed to the reduction of spin-orbit strength.

After this experiments Time Domain Spectroscopy for measuring the THz signal we performed at Laboratoire Pierre Agrain (LPA) in Paris. In this case samples have 2nm-thick Co layer. Results are shown in figure 3.5.

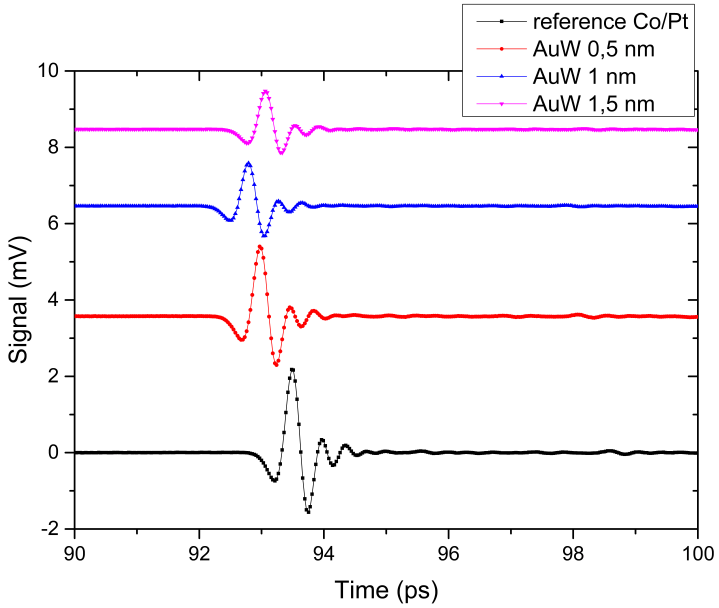

FIGURE 3.5 THz emission for Co(2nm)/Au(t)/Pt(4nm) samples

THz signal can be evaluate taking into account the peak-to-peak value. This value decreases by increasing the Au thickness, as it's possible to note from the table 3.2 below.

TABLE 3.2 Peak-to-peak values for THz emission

Samples	Peak to peak value (mV)
Co(2)/Pt(4) (reference)	3.74
Co(2)/AuW(0,5)/Pt(4)	3.11
Co(2)/AuW(1)/Pt(4)	1.91
Co(2)/AuW(1.5)/Pt(4)	1.61

The significant conclusion is that the THz signal follow the behavior of the spin mixing conductance, it decreases by increasing the Au thickness. Even if the Inverse Spin Hall has a small increasing trend together with insertion's thickness, for the emission is much more relevant the behavior of the spin mixing conductance. Now it is important to know if this relation is respected also for other samples or not.

3.2 Bilayer Co/Pt with Au:W at the edge

For these samples an higher percentage of tungsten(W) was introduced in Au layer in order to reduce Au spin diffusion length and create a spin-sink back in the Pt layer [19]. It's useful to have more spin current in Pt because it is responsible for the spin to charge conversion only in nonmagnetic material. For this family we have two samples with Pt thicknesses of 2 and 3 nm

respectively and fixed thickness of Au:W (4nm). FMR and ISHE measurements are used like for the first family to extract significant parameters. Values obtained from FMR measurements are reported in the table 3.3 below.

TABLE 3.3 Values extracted from FMR measurements

Sample	Damping value $\Delta\alpha$ (nm^{-2})	M_{eff} (emu/cm^{-3})	$\Delta\alpha \cdot M_{eff}$
Co(10nm)/Pt(4nm) (ref)	0.009983 ± 0.000438	1585.426728	$15.82731503 \pm 0.694416907$
Co(10)/Pt(2)/Au:W(4)	0.010428 ± 0.000144	1487.4045	$15.51065413 \pm 0.214186248$
Co(10)/Pt(3)/Au:W(4)	0.009811 ± 0.000285	1443.153518	$14.15877917 \pm 0.411298753$

In this case the Gilbert damping parameter does not posess a precise behavior but it seems to be almost the same for the different samples. The effective magnetization plays a much important role in determining the decreasing behavior of the product that represents also the behavior of the spin mixing conductance. The product is almost the same (by taking into account also the error bar) for the reference sample and the sample with 2nm-thick Pt and it decreases for the sample with 3nm-thick Pt layer.
ISHE measurements have been performed to check again if the spin to charge conversion normally occurs and to make a comparison among the samples of the same family.

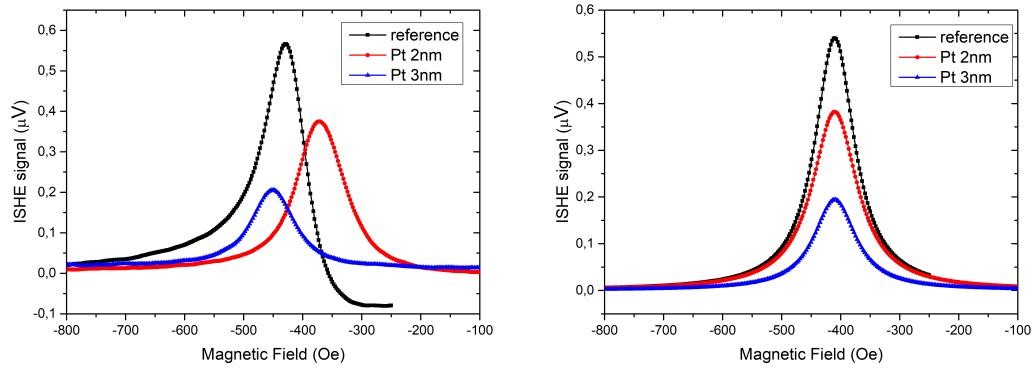

FIGURE 3.6 ISHE signal for negative field: measured data on left and symmetric part with same resonant field on right

Measurements reported in figure 3.6 show that new samples have lower ISHE signal with respect to the reference Co/Pt bilayer with an higher signal between the two for the 2 nm-thick Platinum sample. This appears contradictory, at the first view, because the only thing that changes is the Pt thickness but not his spin diffusion length.
The last step is THz measurement, performed on analog samples but with 2nm-thick Cobalt layer instead of 10 nm Co-samples used for both FMR and ISHE. Results are reported below in fig 3.7 and table 3.4.

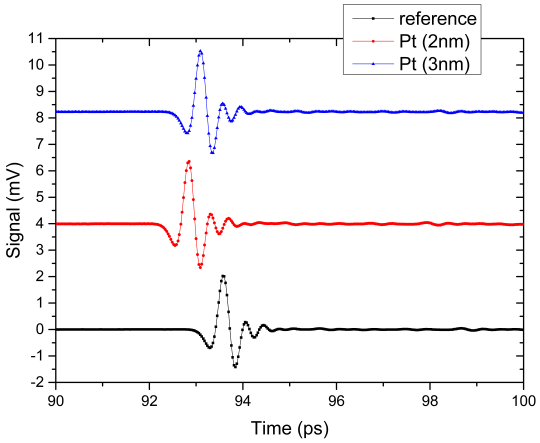

FIGURE 3.7 THz emission for Co/Pt(t)/AuW samples

TABLE 3.4 Peak-to-peak values for THz emission

Samples	Peak to peak value (mV)
Co(2)/Pt(4)	3.74
Co(2)/Pt(2)/AuW(4)	4.01
Co(2)/Pt(3)/AuW(4)	3.85

THz signal is higher for the 2 samples of this family than for the reference. To better understand what is the relationship between the THz signal and the spin mixing conductance, more properly the product $\Delta\alpha \cdot M_{eff}$, a plot with error bars has been drawn in fig 3.8. The product has been normalized with respect to the reference value.

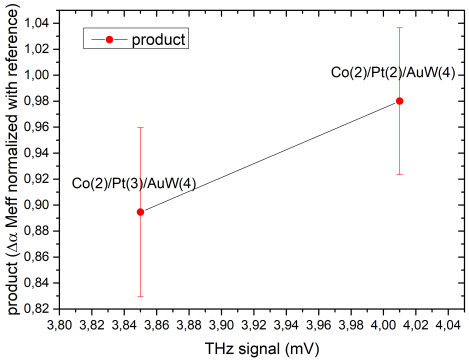

FIGURE 3.8 Reciprocal behavior of product $\Delta\alpha \cdot M_{eff}$ (normalized with respect to the same product value but for the reference) with respect to the THz behavior

Even if the number of sample is small, for this particular series, the relationship between the spin-mixing conductance and the THz signal is still preserved and increasing $g_{eff}^{\uparrow\downarrow}$ the THz signal increases as well.

3.3 Bilayer Co/Pt with insertion of Ti-monolayer

The idea behind this family of samples is the same than the first one: to insert an intermediate layer in between Cobalt and Platinum to reduce the spin memory loss at interface but in this case using Titanium monolayers. For this category, other two samples were fabricated with Ti thickness of 0.4 nm and 0.8 nm. The procedure is always the same so first of all FMR was performed to extract the parameters values reported in table 3.5.

TABLE 3.5 Values extracted from FMR measurements

Ti thickness (nm)	Damping value $\Delta\alpha$ (nm^{-2})	M_{eff} (emu/cm^3)	$\Delta\alpha \cdot M_{eff}$
$0(Co/Pt)$	0.016428 ± 0.001503	1429.783833	$23.48848881 \pm 2.148965101$
0.4	0.009933 ± 0.00063	1339.367179	$13.30393419 \pm 0.843801323$
0.8	0.008217 ± 0.000501	1437.500149	$11.81193872 \pm 0.720187575$

The behavior of the spin mixing conductance is exactly the same with respect to the one with Au family, it decreases by increasing the thickness of Titanium insertion. As usual the next step has consisted in ISHE measurements, fig. 3.9 shows the results in which it's possible to see that signal decreases by increasing Ti thickness. These results are opposite with respect to the ones obtained for Au family in this work and they are contradictory with respect to the others obtained in Korea [13] with CoFeB/Pt bilayer and Ti insertion in between.

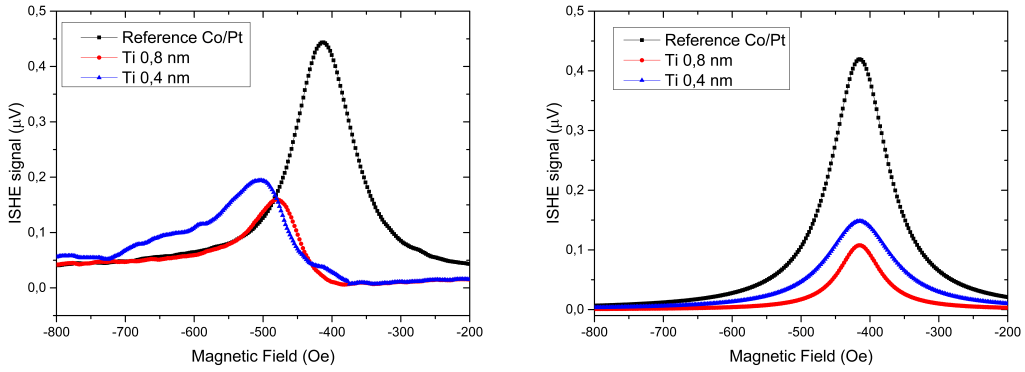

FIGURE 3.9 ISHE signal for Co/Ti(t)/Pt

Previous measurements presented in this manuscript suggest that if Ti thickness increases the signal in THz domain should decrease as well. Time Domain Spetroscopy is used to verify if expectations are corrected or not (results in fig. 3.10 and table 3.6).

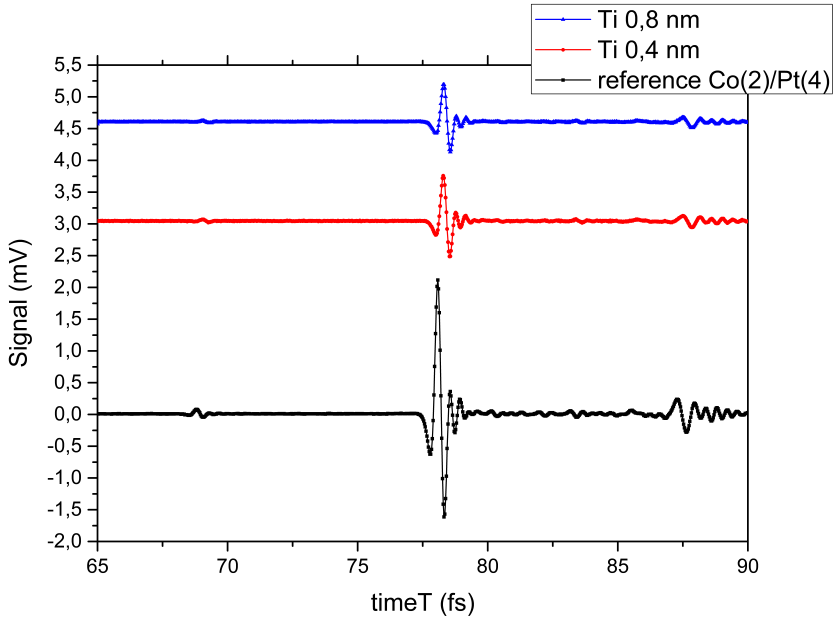

FIGURE 3.10 THz emission for Co/Ti(t)/Pt samples

TABLE 3.6 Peak-to-peak values for THz emission

Samples	Peak to peak value (mV)
Co(2)/Pt(4)	3.74
Co(2)/Ti(0.4)/Pt(4)	1.27
Co(2)/Ti(0.8)/Pt(4)	1.061

Expectations are well respected since the THz signal decreases clearly as for the spin mixing conductance by increasing the thickness of Ti layer. The observed tendency is different with respect to the reference ([13]) surely because Ti deposition is not performed in the same conditions in the two cases.

3.4 Bilayer Co/Pt with Ru at the edge

This series is composed by samples with four different combinations of Pt and Ruthenium(Ru) together with the classical ferromagnetic Co layer: Co/Pt(4nm)/Ru(4nm), Co/Pt(4nm)/Ru(3nm), Co/Pt(3nm)/Ru(4nm) and Co/Pt(3nm)/Ru(3nm). Ru plays the role of spin-sink avoiding spin back-flow (reflection) at the outward interface. The configuration used in this case has been chosen by looking at very good emission obtained for the second family. The only change is the use of Ru layer instead of gold one to complete the stricture.
FMR measurments have been performed on samples with Cobalt's thickness of 10 nm and extracted values are collected in table 3.7.

TABLE 3.7 Values extracted from FMR measurements

Sample	Damping value $\Delta\alpha$ (nm^{-2})	M_{eff} (emu/cm^3)	$\Delta\alpha \cdot M_{eff}$
Co(10)/Pt(4) (reference)	0.007855 ± 0.000634	1499.673413	$11.77993466 \pm 0.950792944$
Co(10)/Pt(4)/Ru(4)	0.008077 ± 0.000437	1566.831833	$12.65530072 \pm 0.684705511$
Co(10)/Pt(4)/Ru(3)	0.008959 ± 0.000687	1550.256308	$13.88874626 \pm 1.065026084$
Co(10)/Pt(3)/Ru(4)	0.009666 ± 0.001023	1548.99314	$14.97256769 \pm 1.584619982$
Co(10)/Pt(3)/Ru(3)	0.009932 ± 0.000869	1582.150059	$15.71391439 \pm 1.374888401$

By this way, it's possible to see how the spin mixing conductance changes for the different thickness. In general the sample with 3nm-thick Platinum have higher $g_{eff}^{\uparrow\downarrow}$ with respect to 4nm-thick Pt ones and then for samples with same Platinum's thickness the higher values are reached for 3nm-thick Ruthenium samples.
The second step is to measure the ISHE signal for all the samples. The results are shown in fig.3.11. All the signals are lower with respect to the reference and it's interesting to note that in this family all amplitudes are comparable each other with small differences. The best sample for ISHE is, as expected, the sample with larger Platinum and Ruthenium layers because this means that the region in which the spin to charge conversion takes place is larger.

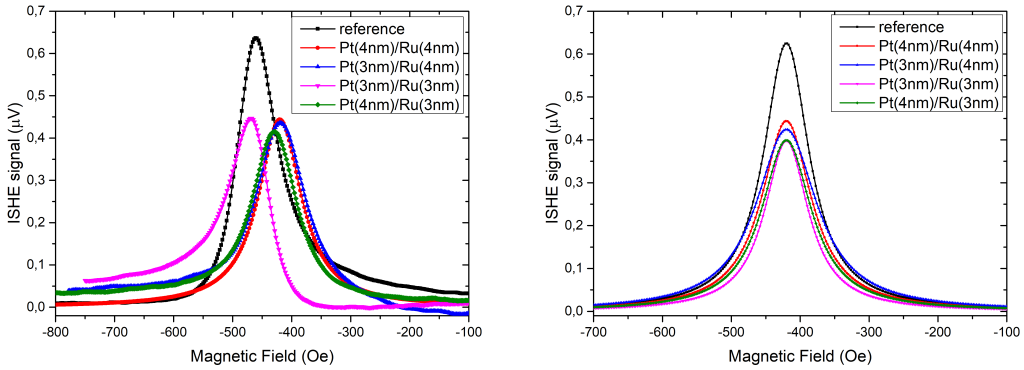

FIGURE 3.11 ISHE signal for Co/Pt(t1)/Ru(t2)

Once resuts from FMR and ISHE are calculated, last step is to perform Time Domain Spectroscopy with samples that have 2nm-thick Cobalt layer to analyse how the THz signal changes (fig 3.12 and table 3.8).

Peak to peak values show that for the sample in this sample again we have an high signal for the one with larger product $\Delta\alpha M_{eff}$, representative of the behavior of spin mixing conductance. Fig 3.13 collects the relationship between the two, where on y-axis the product values have been normalized with respect to the value obtained for the reference sample. These results are reasonable with respect to the ones measured with the other families.

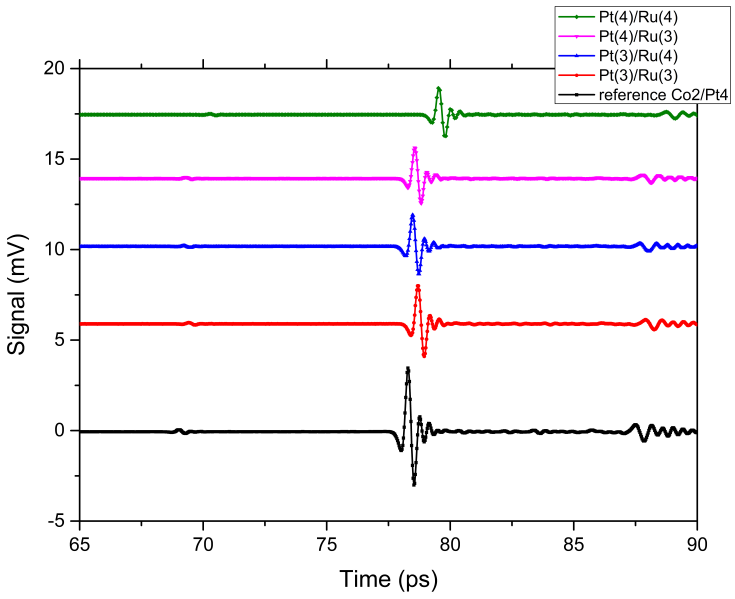

FIGURE 3.12 THz emission for Co/Pt(t1)/Ru(t2) samples

TABLE 3.8 Peak-to-peak values for THz emission

Samples	Peak to peak value (mV)
Co(2)/Pt(4)	6.4686
Co(2)/Pt(3)/Ru(3)	3.8942
Co(2)/Pt(3)/Ru(4)	3.269
Co(2)/Pt(4)/Ru(3)	3.064
Co(2)/Pt(4)/Ru(4)	2.6436

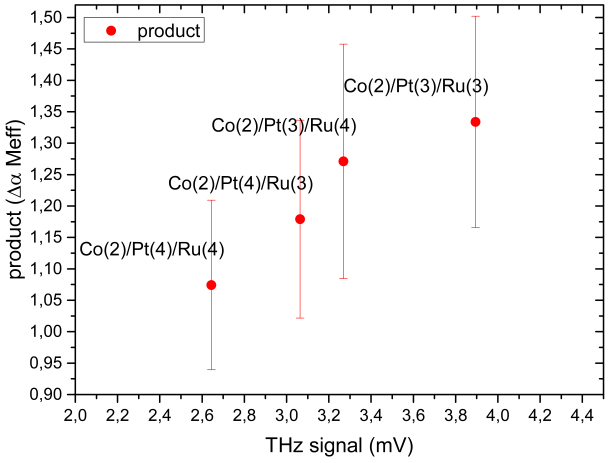

FIGURE 3.13 Relationship between spin mixing conductance behavior and THz peak-to-peak values

CHAPTER 4

Theory and Simulations

This chapter is devoted to Theory and simulations. The focus is on generation and diffusion profile of spin current induced in bilayers by laser excitation. This investigation is in the steady state regime, equivalent to continuous wave excitation.

4.1 Steady State without spin orbit: reference code

During the internship home-made transport calculation codes were used that compute step for the spin orbit transport at interface for both bilayer and trilayer. They implements the scattering formalism(theoretical section) applied to chosen structure. A comparison can be done with the diffusive method described in [20] (Fert-Jaffrés model) for the a system composed by a ferromagnetic layer and a semiconductor. In particular for this model the value of the spin polarization at the interface is:

$$SP = \frac{\beta \cdot r_{FM} + \gamma r_b}{r_{FM} + r_{NM} + r_b}$$

where r_{FM} is the resistance (per unit area) in the ferromagnetic layer, r_{NM} resistance(per unit area) in non magnetic layer, β is the spin asymmetry in ferromagnetic bulk, γ is the spin asymmetry coefficient that depend on interface quality, r_b is the resistance (per unit area) introduced by the interface. By considering that $\gamma = 0$ we have:

$$SP = \frac{\beta}{1 + \frac{r_{NM}+r_b}{r_{FM}}}$$

with the ratio $\frac{r_{NM}}{r_{FM}} = \frac{l_{sd,NM}}{\lambda_{NM}} \cdot \frac{\lambda_{FM}}{l_{sd,FM}}$ where l_{sd} is the spin diffusion length and λ is the mean free path in each region. Since these data are saved in a file it's possible to change alternately spin diffusion length or mean free path (in order to produce a variation in their ratio and so in the resistances) in one or the other material and run the code by considering the case in which there is no spin-orbit interaction to see how the spin polarization changes at the interface. The results (fig 4.1 and 4.2) show that effectively the spin polarization at interface depends only by the ratios r_{FM} and r_{NM}. From the different values of SP extracted from the simulations it's possible to extract the value for the average transmission coefficient at the interface $\bar{T}$ ($r_b = \frac{1}{\bar{T}}$) that results

to be $\bar{T} = 0.52028$ for all the possible ratios with the chosen parameters (electronic wavevector in the FM and SOC layers mainly). With this value obtained for interface transmission a direct comparison between diffusive model and scattering one can be computed and the results for both are in complete agreement one with respect to the other.

These simulations and results are very interesting because they put in evidence the developped spin orbit transport code has general validity and it includes also the situation of the diffusive model when there is no spin orbit interaction at the interface.

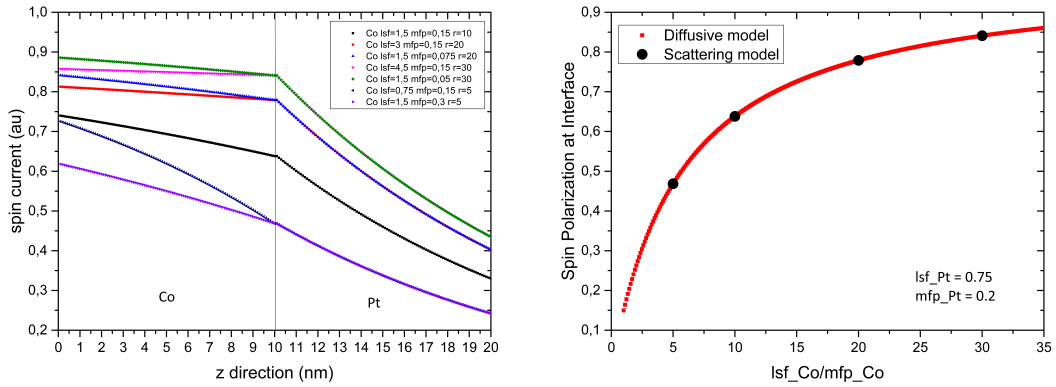

FIGURE 4.1 (Left Panel) Spin polarization profile in z for the structure Co(10nm)/Pt(10nm) by varing the resistance in Co side with no spin orbit interaction. (Right panel) Extracted values of spin polarization at the interfaceby changing the ratio $\frac{l_{sd,Co}}{\lambda_{Co}}$ with both scattering (black dots) and diffusive model (red dots). Values of spin diffusion length (lsf) and mean free path (mfp) are expressed in the order of Copper mean free path ($= 20nm$). Pt parameters are lsf=15nm and mfp=4nm.

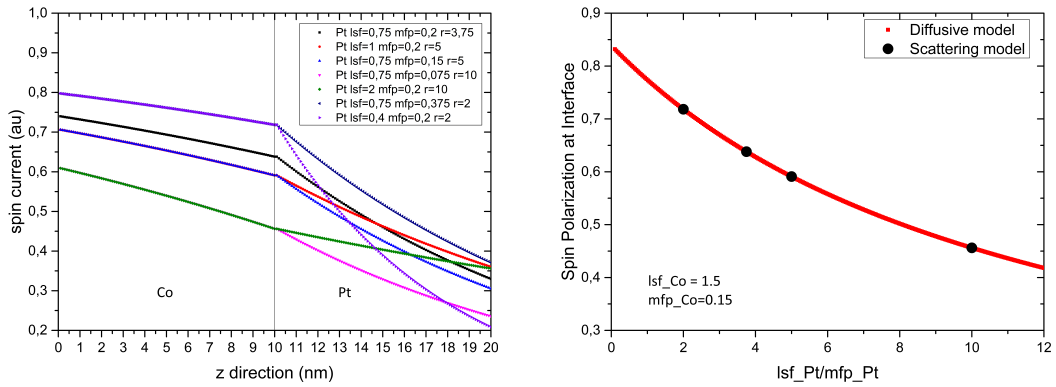

FIGURE 4.2 (Left Panel) Spin polarization profile in z for the structure Co(10nm)/Pt(10nm) by varing the resistance in in Platinum side with no spin orbit interaction. (Right panel) Extracted values of spin polarization at the interface by changing the ratio $\frac{l_{sd,Pt}}{\lambda_{Pt}}$ with both scattering (black dots) and diffusive model (red dots). Values of spin diffusion length (lsf) and mean free path (mfp) are expressed in the order of Copper mean free path ($= 20nm$). Co parameters are lsf=30nm and mfp=3nm.

4.2 General case: steady state involving spin-orbit interactions

The numerical procedure computed by codes is linked to the theoretical introduction of this manuscript, in the treatment of spin orbit transport involving, now, Rashba interactions. At the interface the Bloch periodicity (that is valid in bulk regions) is broken and this is expressed by the presence of a Dirac function in the Hamiltonian. For the description of the behavior at the interface it's possible to use the scattering matrix formalism with spinors: this means that reflection and transmission are 2x2 matrices and scattering matrix becomes a 4x4 matrix [21].

$$\begin{pmatrix} \Psi^{1x2}_{out,L} \\ \Psi^{1x2}_{out,R} \end{pmatrix} = \hat{S} \begin{pmatrix} \Psi^{1x2}_{inp,L} \\ \Psi^{1x2}_{inp,R} \end{pmatrix} = \begin{pmatrix} \hat{r}^{2x2} & \hat{t}'^{2x2} \\ \hat{t}^{2x2} & \hat{r}'^{2x2} \end{pmatrix} \begin{pmatrix} \Psi^{1x2}_{inp,L} \\ \Psi^{1x2}_{inp,R} \end{pmatrix}$$

where Ψ indicates spinors that could be as input or output and at left or at right (left and right can be nonmagnetic or ferromagnetic material reciprocally), r and t (r' and t') represent reflection and transmission matrices for spinor incoming from left (right). To calculate all the values of $\hat{S}$-matrix boundary conditions have to be satisfied: the continuity of the spinors ($\Psi_{FM} = \Psi_{NM}$) and current-wave ($\hat{J}\Psi_{FM} = \hat{J}\Psi_{NM}$) at the interface, where charge current operator is $\hat{J} = \frac{\partial \hat{H}}{\partial \hat{k}} + 2iU\Theta(x)$. Then it's possible to evaluate the spin current operator to calculate what are the expectation values for both charge and spin currents. Without Rashba interactions ($U = 0$) both currents are continous at the interface; the introduction of the SOI term breaks the continuity for the spin current. This developpement is obtained working in equilibrium conditions. To have a full model that describes the situation with also spin accumulation it's possible to start from the equilibrium case adding some perturbation terms to the different currents. If a the begging the spin currents are $J^+_{0L}, J^-_{0L}, J^+_{0R}, J^-_{0R}$ there are perturbative terms $\delta J^+_{0L}, \delta J^-_{0L}, \delta J^+_{0R}, \delta J^-_{0R}$ directly realted to spin accumulation through the precessing upward/downward matrix $\alpha^{+/-}$ ($\delta\mu_{4x1} = \hat{\alpha}^{+/-}_{4x4}\delta J_{4x1}$). With these new terms new boundary condition are necessary that involve also equilibrium paramenters, reflection and trasmission matrices (4x4 matrces in this case) and precessing upward and downward [21]:

$$\begin{pmatrix} (\hat{1}_{4x4} + \hat{r}) + (\hat{1} - \hat{r})\hat{\alpha}^-_L & t'(\hat{1} - \hat{\alpha}^+_R) \\ \hat{t}(\hat{1} - \hat{\alpha}^-_L) & (\hat{1} + \hat{r}') + (\hat{1} - \hat{r}')\hat{\alpha}^+_R \end{pmatrix} \begin{pmatrix} \delta J^-_L \\ \delta J^+_R \end{pmatrix} =$$

$$\begin{pmatrix} \hat{1} + \hat{r} & \hat{t}' \\ \hat{t} & \hat{1} + \hat{r}' \end{pmatrix} \begin{pmatrix} J^+_{0L} - J^-_{0L} \\ J^-_{0R} - J^+_{0R} \end{pmatrix} + \begin{pmatrix} (\hat{1}_{4x4} + \hat{r}) - (\hat{1} - \hat{r})\hat{\alpha}^+_L & \hat{t}'(\hat{1} + \hat{\alpha}^-_R) \\ t(\hat{1} + \hat{\alpha}^+_L) & (\hat{1} + \hat{r}') - (\hat{1} - \hat{r}')\hat{\alpha}^-_R \end{pmatrix} \begin{pmatrix} \delta J^+_L \\ \delta J^-_R \end{pmatrix}$$

This boundary equation, together with the unitary property of the scattering matrix ensures the continuity of charge current at the interface. Nevertheless spin current can have discontinuity at the interface so there is still the possibility to have Spin Memory Loss.

Scattering mechanism is very useful because in this way it's possible to model also systems with more than a single interface. Codes have been used to better understand the influence of some

parameters, like for example the Rashba spin orbit interaction at interface in the studied devices. In this case in fact it's possible to see that if the spin orbit interaction is zero at interface not only the charge current is constant but also the spin current, if spin orbit increases the spin current show a discontinuity at interface and charge current remains constant, as explained in the theoretical introduction (fig 4.3). This is exactly the reason why putting gold in between Cobalt and Platinum: this insertion should reduce SOI and so the spin memory loss should decrease, increasing the spin current injected in Platinum layer.

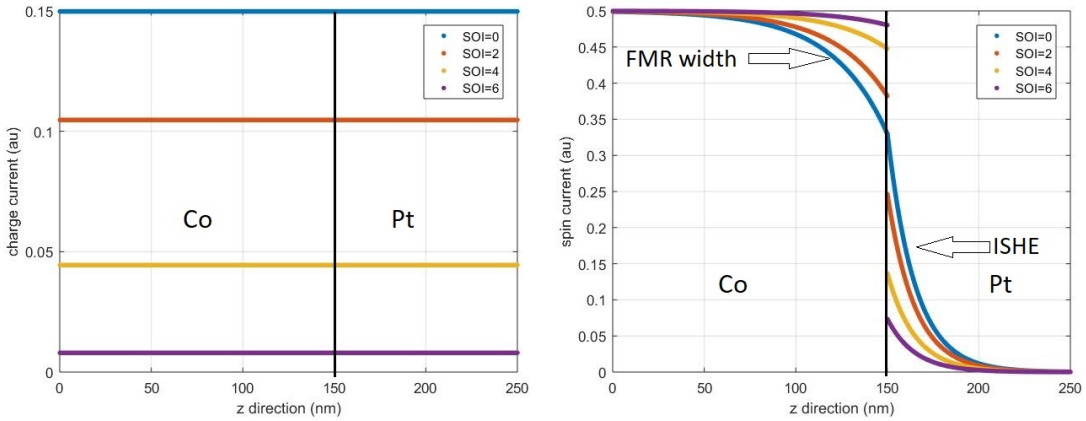

FIGURE 4.3 Charge current (left) and spin current (right) profiles in the structure Cobalt (150nm)/Pt(100nm) by varying the Rashba interaction at the interface (in term of spin orbit wavevector, SOI is in nm^{-1}). For this simulation we fix the spin current polarization in Co at 0.5 and diffuison lengths at 15 nm for Pt and 30 nm for Co

The code is built to describe the spin pumping experiments due to magnetization dynamics in the ferromagnet. In particular when the spin orbit is present at interface the value of spin polarization from the ferromagnetic side gives an idea of the amplitude of FMR signal of that sample, the area under the spin polarization curve into the nonmagnetic material is related to the ISHE signal (as evidenced in right panel of figure 4.3). A possible improvement of the code will be to include also time domain excitation due to femtosecond laser pulse in order to better understand the results obtained for THz emission.

CHAPTER 5

Conclusions and perspectives

Among the different series that have been test a way was found that can really produce an increasing in the emitted signal, by placing a spin absorber like Au:W in contact with Platinum and reducing the dimensions of Pt itself. This way could be followed with much more samples with different layer thicknesses to have a picture of what is the best to do for larger THz signal. An idea, for example could be to work with materials with high spin mixing conductance like topological insulators (e.g. α-Sn).

Measurements show that for all the samples that belong to a specific family there is a proportionality for which at higher values of spin mixing conductance correspond higher values of THz amplitudes. For the comparison with the reference is important to underline that becomes important also the evaluation of the spin hall angle in the structures. For example in the last family the value of the spin mixing conductance is higher with respect to the reference for all samples but the THz signal is always lower. This result can be understood by taking into account that in this model THz amplitudes are proportional to spin mixing conductance, spin hall angle and spin diffusion length ($A_{THz} \propto g_{eff}^{\uparrow\downarrow} \cdot \theta_{SHE} \cdot l_{sd}$) but in a first approximation latter two are taken as constants. In reality there could be some changes due to the differences among the configurations that play a crucial role in determining the signal amplitude. Next steps could be to include in this model also the evaluation of the spin hall angle to have a complete picture of the situation, by introducing an effective spin hall angle $\theta_{ISHE,eff}$. This could allow to understand a complete methodology to find optimized structures (starting with the famous Co/Pt) with higher THz signals.

In the next future there will be some attempts to perform Time Domain Spectroscopy measurements at low temperature to see how THz signal changes, due to the fact that in theory spin mixing conductance and spin diffusion length should increase by reducing the temperature.

Bibliography

[1] Y. Wu, M. Elyasi, X. Qiu, M. Chen, Y. Liu, L. Ke, and H. Yang, "High performance thz emitters based on ferromagnetic/nonmagnetic heterostructures," *Adv Materials*, vol. 29, 2016.

[2] T. Seifert, S. Jaiswal, U. Martens, J. Hannegan, L. Braun, and al, "Efficient metallic spintronic emitters of ultrabroadband terahertz radiation," *Nature Photonics*, vol. 10, May 2016.

[3] D.Yang, J. Liang, C. Zhou, L. Sun, R. Zheng, S. Luo, Y. Wu, and J. Qi, "Powerful and tunable thz emitters based on the fe/pt magnetic heterostructure," *Advanced Materials*, vol. 4, pp. 1944–1949, 2016.

[4] J. R. Sanchez, N.Reyren, P.Laczowski, H. Jaffrés, and J.-M. George, "Spin pumping and inverse spin hall effect in platinum: The essential role of spin memory loss at metallic interfaces," *Physical Review Letters*, vol. 112, p. 106602, 2014.

[5] R. Iguchi and E. Saitoh, "Measurements of spin pumping voltage separeted from extrinsic microwave effects," *Journal of the Physical Society of Japan*, vol. 86, 2016.

[6] H. Jaffrès, T.-H. Dang, Q. Barbedienne, J.-M. George, N. Reyren, S. Collin, P. Bortolotti, H. Nong, J. Tignon, S. Dhillon, L. Divay, L. Vila, and P. Noël, "Spin-hall effects and unconventional anomalous hall effects in transition-metal based metallic spintronic multilayers for thz emission," in *SPIE Spintronics XI*, San Diego, California USA, 2018.

[7] H. Jaffrès, J.-M. George, N. Reyren, S. Collin, P. Bortolotti, S. Dhillon, and al, "Spinorbitronics at interfaces for thz emission," in *Material Sciences Engineering, conferenceseries*, Barcelona, Spain, 2018.

[8] T.-H. Dang, H. Jaffrès, Q. Barbedienne, V. Volpe, H. Nong, J. Hawecker, J. Tignon, N. Reyren, J.-M. George, L. Vila, S. Collin, P. Bortolotti, and S. Dhillon, "Spin-hall effects in 3d/5d transition-metal based multilayers for thz emission," in *IEEE-Intermag*, Singapore, 2018.

[9] M.Perenzoni and J. Paul, *Physics and Applications of Terahertz Radiation*. Springer, 2014.

[10] J. W. Han, S. Y. Hamh, T. H. Kim, K. S. Lee, N. E. Yu, D.-K. Ko, and J. S. Lee, “Extraction of optical constants using multiple reflections in the terahertz emitter-sample hybrid structure,” *IEEE transactions on electron devices*, vol. 54, pp. 921–931, May 2007.

[11] Z. Jin, A.Tkach, F.Casper, and al, “Accessing the fundamentals of magnetotransport in metals with terahertz probes,” *Nature Physics*, vol. 11, p. 761, 2015.

[12] P. Laczkowski, J.-C. Rojas-Sánchez, W. Savero-Torres, H. Jaffrès, and N. Reyren, “Experimental evidences of a large extrinsic spin hall effect in auw alloy,” *Applied Physics Letters*, vol. 104, 2014.

[13] H.-Y. Lee, S. Kim, J.-Y. Park, Y.-W. Oh, and al, “Enhanced spin-orbit torque via interface engineering in pt/cofeb/mgo heterostructures,” *Not yet published*, 2018.

[14] Y.Tserkovnyak, A.Braatas, and G. Bauer, “Spin pumping and magnetization dynamics in metallic multilayers,” *Physical Review Letter*, vol. 88, 2002.

[15] M.Battiato, K.Carva, and P. Oppeneer, “Theory of laser-induced ultrafast superdiffusive spin transport in layered heterostructures,” *Physical Review B*, vol. 86, 2012.

[16] E. Beaurepaire, J.-C. Merle, A. Daunois, and J.-Y. Bigot, “Ultrafast spin dynamics in ferromagnetic nickel,” *Physical review letters*, vol. 76, May 1996.

[17] T. Valert and A. Fert, “Theory of the perpendicular magnetoresistance in magnetic multilayers,” *Physical Review B*, vol. 48, pp. 7099–7113, 1993.

[18] C. Kittel, “On the theory of ferromagnetic resonance absorption,” *Phys. Rev.*, vol. 155, p. 155, 1948.

[19] X. Qiu, W. Legrand, P. He, Y. Wu, and J. Yu, “Enhanced spin-orbit torque via modulation of spin current absorption,” *Physical Review Letters*, vol. 117, 2016.

[20] A. Fert, H. Jaffrès, J.-M. George, and R.Mattana, “Semiconductors between spin-polarized sources and drains,” *IEEE transactions on electron devices*, vol. 39, pp. 921–931, May 2007.

[21] T. Deng and H. Jaffrès, “Spin-polarized and spin-orbit transport at metallic interfaces including spin-orbit interactions,” *Unpublished work*.